Journal of Statistical Physics, Vol. 90, Nos. 3/4, 1998

First-Order Phase Transitions in One-Dimensional Steady States

Peter F. Arndt,[1,2] Thomas Heinzel,[1,2] and Vladimir Rittenberg[1,2]

Received July 31, 1997; final November 6, 1997

The steady states of the two-species (positive and negative particles) asymmetric exclusion model of Evans, Foster, Godrèche, and Mukamel are studied using Monte Carlo simulations. We show that mean-field theory does not give the correct phase diagram. On the first-order phase transition line which separates the *CP*-symmetric phase from the broken phase, the density profiles can be understood through an unexpected pattern of shocks. In the broken phase the free energy functional is not a convex function, but looks like a standard Ginzburg–Landau picture. If a symmetry-breaking term is introduced in the boundaries, the Ginzburg–Landau picture remains and one obtains spinodal points. The spectrum of the Hamiltonian associated with the master equation was studied using numerical diagonalization. There are massless excitations on the first-order phase transition line with a dynamical critical exponent $z = 2$, as expected from the existence of shocks, and at the spinodal points, where we find $z = 1$. It is the first time that this value, which characterizes conformal invariant equilibrium problems, appears in stochastic processes.

KEY WORDS: Stochastic lattice gas; phase transitions; shocks; spinodal points; spontaneous symmetry breaking; free energy functional.

1. INTRODUCTION

Several years ago Krug[1] suggested the existence of boundary induced phase transitions in one-dimensional steady states. A line of first-order phase transitions (the so-called coexistence line) was found in the one-species asymmetric exclusion model[2,3,4] in which particles (call them positive) hop among vacancies (call them negative particles). On the coexistence line, the system is *CP*-symmetric (*C* corresponds to changing

[1] SISSA, 34014 Trieste, Italy.
[2] Physikalisches Institut, 53115 Bonn, Germany.

0022-4715/98/0200-0783$15.00/0

the sign of the particles, P is the parity operation) and the symmetry is spontaneously broken (some aspects of this phase transition which are relevant to this paper are reviewed in Appendix A). Since we want to compare the nature of the phase transitions in equilibrium and non-equilibrium phenomena, the phase transition just described would correspond to the two-dimensional n-state Potts model[5] with $n>4$ at the critical temperature. The exclusion model does not have the equivalent of the low temperature domain which corresponds to the broken phase.

The two-species model of Evans, Foster, Godrèche and Mukamel[6, 7] presents a broken phase (the equivalent of the low temperature domain of the n-states Potts models) and this motivated us to study this model in detail. In our investigation we got a few surprises.

We will just reproduce from ref. 7 the definition of the model, introducing also symmetry breaking boundary terms, and send the reader to the same paper in order to find out why the model is physically relevant. Each site of a one-dimensional lattice with L sites may be occupied by a positive particle or a negative particle or be empty. In each infinitesimal time step dt the following events may occur at each nearest-neighbor sites $k, k+1$:

$$\begin{aligned} (+)_k (0)_{k+1} &\to (0)_k (+)_{k+1} \\ (+)_k (-)_{k+1} &\to (-)_k (+)_{k+1} \\ (0)_k (-)_{k+1} &\to (-)_k (0)_{k+1} \end{aligned} \tag{1.1}$$

all with probability dt. Where $(+)_k$, $(-)_k$ and $(0)_k$ indicate a positive particle, a negative particle or a vacancy at the site k. In the same time step dt the following events may occur at the left boundary ($k=1$)

$$\begin{aligned} (0)_1 &\to (+)_1 \quad \text{with probability} \quad \alpha\, dt \\ (-)_1 &\to (0)_1 \quad \text{with probability} \quad \beta(1-h)\, dt \end{aligned} \tag{1.2}$$

and at the right boundary ($k=L$)

$$\begin{aligned} (0)_L &\to (-)_L \quad \text{with probability} \quad \alpha\, dt \\ (+)_L &\to (0)_L \quad \text{with probability} \quad \beta(1+h)\, dt \end{aligned} \tag{1.3}$$

One notices that for $h=0$ the probabilities are CP-invariant, the case h bigger than zero will be considered in Section 4.

The time evolution of the system is given by a master equation or its equivalent imaginary time Schrödinger equation[8]

$$\frac{d}{dt}|P\rangle = -H|P\rangle \tag{1.4}$$

where $|P\rangle$ is the probability vector and H is the hamiltonian of a one-dimensional quantum chain which is given in Appendix B. For most of this paper we will be interested in the properties of the steady state.

Let us introduce some notations: $p(k)$, $m(k)$ and $v(k)$ will denote the steady state density of positive, negative particles and vacancies at the site k. Their average values being p, m respectively v. It is also useful to define the quantities

$$\begin{aligned} d(k) &= p(k) - m(k) \\ s(k) &= (p(k) + m(k))/2 \end{aligned} \tag{1.5}$$

their average values being d and s.

The phase diagram corresponding to the steady state was obtained in mean-field theory for the CP-symmetric case[7] and is shown in Fig. 1. One distinguishes four phases, we will give the average densities of particles in each one. The power law phase (A):

$$p = m = \tfrac{1}{2}, \qquad v = 0 \tag{1.6}$$

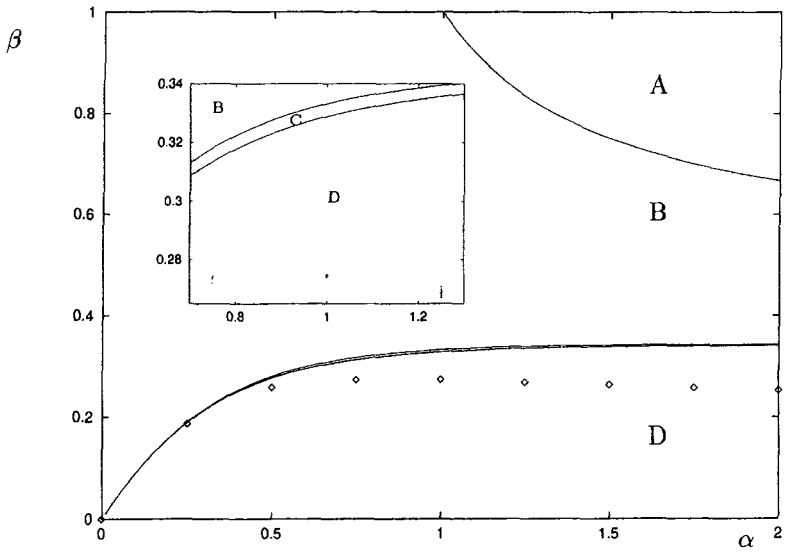

Fig. 1. Phase diagram for $h = 0$. The phases A, B, C and D are obtained in meanfield and defined in the text. Since the C phase is very narrow it is shown in an insert. The diamonds describe the boundary between the phase $\tilde{B}$ and the phase $\tilde{D}$ as obtained in Monte Carlo simulations. (No phase C is observed.)

The low densities ($p = m < 1/2$) symmetric phase (B):

$$p = m = \frac{\alpha\beta}{\alpha + \beta} < \frac{1}{2} \tag{1.7}$$

The low densities ($p, m < 1/2$) broken phase (C): Here mean-field gives three solutions, A symmetric unstable solution

$$p = m = \frac{\alpha\beta}{\alpha + \beta} < \frac{1}{2} \qquad \text{(unstable)} \tag{1.8}$$

and two stable solutions

$$\begin{aligned} s &= 2\left(1 - \frac{\alpha\beta}{\alpha - \beta}\right) \\ d &= \pm 2\left[(s-1)\left(\frac{\alpha\beta}{\alpha - \beta} - s\right)\right]^{1/2} \end{aligned} \tag{1.9}$$

The low density/high density phase (D): mean-field gives again three solutions. A symmetric unstable one which is again described by equation (1.8) like in phase C, a second solution in which the positive particles have a high density ($p > 1/2$) and the negative particles have a low density ($m < 1/2$):

$$\begin{aligned} p &= 1 - \beta \\ m &= \frac{1 + \alpha}{2} - \frac{1}{2}\left[(1 + \alpha)^2 - 4\alpha\beta\right]^{1/2} \end{aligned} \tag{1.10}$$

and a third solution in which in Eq. (1.10) p is exchanged with m. For reasons which will become apparent immediately we have checked which solutions are stable with respect to the mean-field dynamics.

In mean-field theory the transitions between the phases A and B respectively B and C are continuous and the transition between C and D is first-order.

An exact calculation[7] using the matrix product ansatz for the wave function on the line $\beta = 1$ has confirmed the existence of phases A and B. Limited Monte Carlo simulations[7] showed a strong similarity between the true and mean-field phase diagrams for $\alpha = 1$. Since for the two-species model[2–4, 9, 8] the phase diagram obtained by mean-field is exact, it might be tempting to conclude that in the present case the mean-field phase diagram is exact.

In Section 2 we show a detailed Monte Carlo analysis of the model with an unexpected result. The D phase exists only up to a line going through the diamonds in Fig. 1 where a first-order phase transition takes place. We will denote the domain under this line by $\tilde{\mathrm{D}}$. The C phase does not exist, the B phase extends down to the $\tilde{\mathrm{D}}$ phase and will be denoted by $\tilde{\mathrm{B}}$ (see Fig. 14). In this picture the role of mean-field is quite perverse. In the $\tilde{\mathrm{D}}$ domain (broken phase) one has the two solutions described by equation (1.10). Above the line of diamonds the system picks up the symmetric unstable solution given by equation (1.8). This solution coincides with the one which defines phase B.

A useful tool in this analysis is played by the free energy functional which is defined as follows:[10] Take an order parameter w and let $P(L, w)$ be the probability to have w for a lattice with L sites. Defining

$$f_L(w) = -\frac{1}{L} \log P(L, w) \tag{1.11}$$

the free energy functional (FEF) is

$$f(w) = \lim_{L \to \infty} f_L(w) \tag{1.12}$$

For equilibrium systems this is a convex function. As we are going to see this is not true for steady states which do not describe Gibbs ensembles. In the $\tilde{\mathrm{D}}$ domain if we take d as order parameter the FEF looks like a Ginzburg–Landau picture in the case of spontaneous breaking of a symmetry.[18] On the first-order transition line separating the phases $\tilde{\mathrm{B}}$ and $\tilde{\mathrm{D}}$ the FEF is convex, looking like the FEF corresponding to a first-order phase transition in equilibrium phenomena. Above the diamond-line the FEF is a convex function with one minimum only. We have also looked at the spectrum of the hamiltonian (see Appendix B) on the separation line. It is gapless with a critical dynamical exponent[11] $z = 2$. This suggests, from the experience with the one-species model, the existence of shocks.[12, 13] The problems of convergence coming from the definition (1.12) are discussed in Appendix A. (Some of the ideas developed here are already in the paper of Bennett and Grinstein[14]).

In Section 3 we study in detail (for $\alpha = 1$) the nature of the first-order phase transition. A novel feature comes from the fact that we have not one but two order parameters (p and m or s and d). In the $p - m$-plane the minima of the FEF lie on a boomerang like figure. We show how this figure can be obtained by an interesting combination of shocks. The existence of shocks allows the prediction of different density profiles which are indeed observed in several Monte Carlo simulations.

In Section 4 we consider the effect of a symmetry breaking term on the process (we take h bigger than zero in Eqs. (1.2–1.3)). We show that the FEFs look like text book Ginzburg–Landau pictures including the existence of spinodal points in the $\tilde{D}$ phase. As is well known[15] such points do not exist in equilibrium phenomena. The meanfield calculations are presented in Appendix C. They are compared here with the Monte Carlo simulations. It looks like mean-field theory gives a good approximation to the data only for small values of β and large values of h.

Moreover, we show that the spectrum of the hamiltonian defined in Appendix B shows massless excitations at the spinodal point with a dynamical critical exponent $z=1$. This is a very surprising result for stochastic processes. This exponent is typical for continuous equilibrium phase transitions. In Section 5 we present our conclusions.

2. THE PHASE TRANSITION BETWEEN THE BROKEN AND UNBROKEN PHASES

In order to clarify the phase structure of the model, let us take $\alpha=1$. (This is a vertical line in Fig. 1). If one wants to compare equilibrium with non-equilibrium phenomena, it is useful to have in mind the two-dimensional n-state Potts model with $n>4$ and interpret the parameter β as a temperature. Mean-field gives the following values of β for the separations among the various phases:

- $\beta=0.3289$ (between phase D and phase C)
- $\beta=0.3333=1/3$ (between phase C and phase B)
- $\beta=1$ (between phase B and phase A)

In order to check the mean-field predictions we have done Monte Carlo simulations to get $f_L(d)$ taking d (the difference between the averages of positive and negative particles) as order parameter.

In Fig. 2 we show our results for $L=400$ and different values of β (all belonging to the D phase). In order to present the data in a clearer way, we have substracted the values of $f_L(0)$ from $f_L(d)$. The data shown in Fig. 2 are interesting for two reasons: the shape of the FEF and the failure of mean-field predictions. First we notice that a dramatic change occurs around $\beta=0.274$. As will be shown below the precise value is $\beta_{\text{crit}}=0.275$. Below β_{crit} the FEF is not a convex function, it has the behavior of a text-book Ginzburg–Landau picture, and shows two minima at the values given by mean-field (see Eq. (1.10) and the definition (1.5)).

At β_{crit} the FEF behaves like the FEF of an equilibrium first-order phase transition. For $\beta>\beta_{\text{crit}}$ the FEF has the expected behavior for a

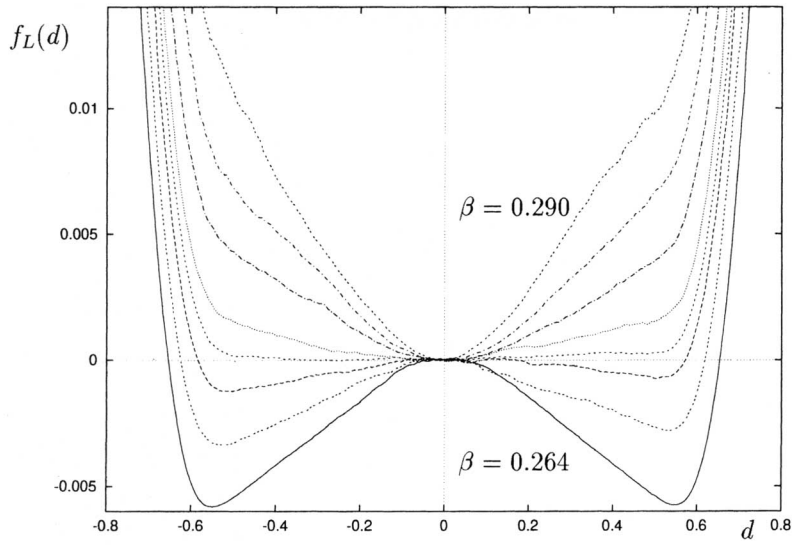

Fig. 2. $f_L(d)$ for $\beta = 0.164, 0.270, 0.274, 0.276, 0.280, 0.285, 0.290$ and $L = 400$ sites. The values of $f_L(d)$ are shifted by their value $f_L(0)$.

disordered phase. Notice that all the changes in the behavior of $f_L(d)$ occur at values of β below the value 0.3289 where, according to mean-field, the transition between the C and D phases is supposed to take place.

In order to make sure that we are not dealing with finite-size effects we have computed $f_L(d)$ for $\beta = 0.3$ (still below 0.3289) for various number of sites up to $L = 1000$. The data are shown in Fig. 3 (we have substracted the value $f_L(0)$). One can see that $f_L(d)$ is practically independent of L (the L dependence is in $f_L(0)$—see Appendix A). This implies that one does not have finite-size effects, and that $f_L(d) - f_L(0)$ is a convex function with one minimum as one expects to have if one is in the "disordered" phase.

We now present more data which show what goes wrong with the mean-field prediction. In Fig. 4 we show the positions of the minima of $f_L(d)$ for various numbers of sites and various values of β. One can observe that below β_{crit} the minima converge to their mean-field values obtained from Eq. (1.10) and that a dramatic change takes place at β_{crit}. Above β_{crit} the CP symmetry is not broken anymore ($d = 0$).

In Fig. 5 we show the minima of $f_L(s)$ as a function of β for various L. The upper curve is given by the average value of s for the two phases (low/high density). This value is obtained from Eq. (1.10):

$$s = \frac{1-\beta}{2} + \frac{1+\alpha}{4} - \frac{1}{4}\left[(1+\alpha)^2 - 4\alpha\beta\right]^{1/2} \tag{2.1}$$

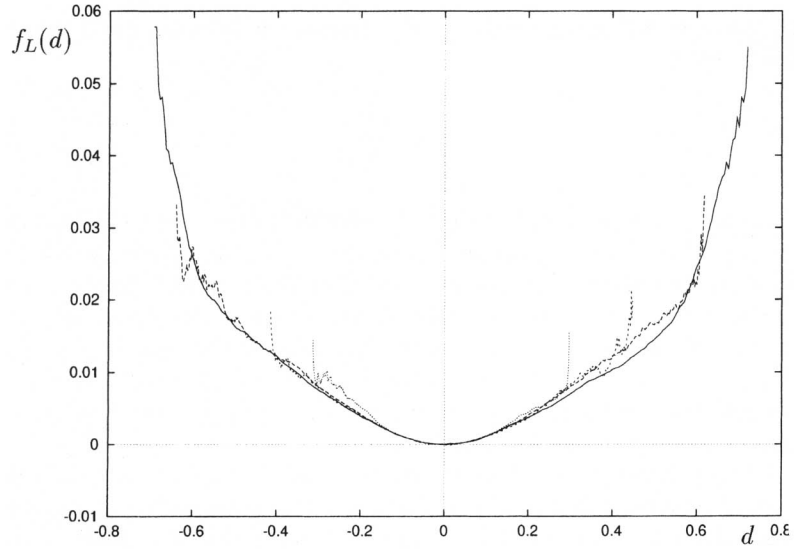

Fig. 3. Free energy functional for $\beta = 0.3$: $f_L(d)$ for $L = 200, 400, 600$ and 1000 sites. The values of $f_L(d)$ for different L are shifted by $f_L(0)$. The little vertical stretches of the curves are due to the limited CPU time of the Monte Carlo runs.

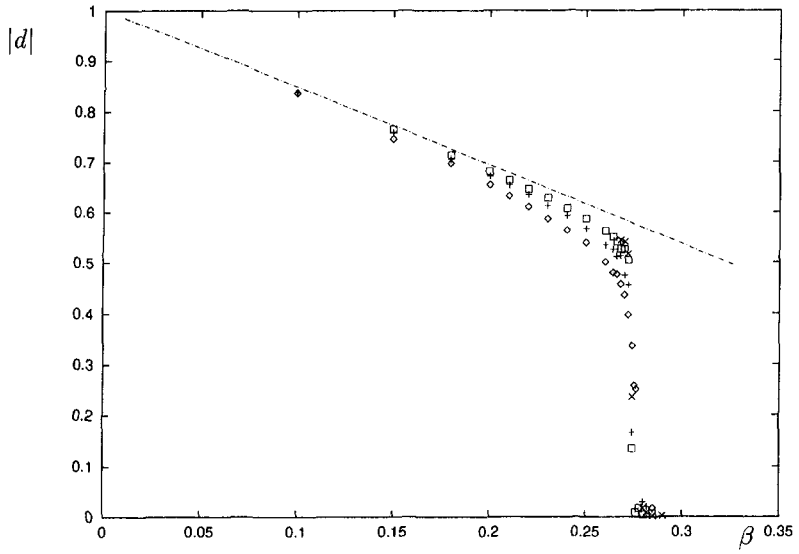

Fig. 4. Minima of $f_L(d)$ for $L = 100$ ($\diamond$), 200 ($+$), 400 ($\square$), 600 ($\times$) sites. The curve ($- \cdot -$) gives the mean-field prediction obtained from Eq. (1.10).

The lower curve corresponds to the symmetric solution (1.8), unstable below $\beta = 1/3$:

$$s = \frac{\alpha\beta}{\alpha + \beta} \tag{2.2}$$

As one can see from Fig. 5, below β_{crit} the data converge to the values of s given by Eq. (2.1) and above β_{crit} to the values of s given by Eq. (2.2). This is very interesting because it means that fluctuations turn the unstable solution into a stable one and one obtains a first-order phase transition. The best estimate for β_{crit} comes from the "fixed point" seen in Fig. 5, one gets $\beta_{\text{crit}} = 0.275 \pm 0.001$ for $\alpha = 1$. By the same method but not with the same patience we have computed the values of β_{crit} for other values of α. The values are given in Table I.

In the correct phase diagram which replaces Fig. 1 one has only three phases: the phase A like in Fig. 1, the phase $\tilde{\text{B}}$ (the unbroken phase) which extends down to the diamond-line in Fig. 1 and finally the phase $\tilde{\text{D}}$ under the diamond-line (see Fig. 14). We have not checked if the seperation between the A and $\tilde{\text{B}}$ phases is properly given by mean-field but we believe

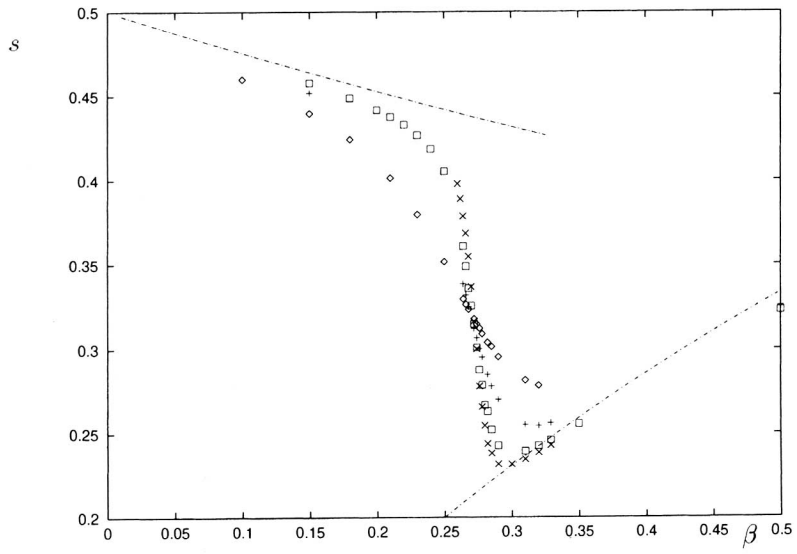

Fig. 5. Minima of $f_L(s)$ ($s = (p+m)/2$) as a function of β for $L = 100$ ($\diamond$), 200 ($+$), 400 ($\square$), 600 ($\times$) sites. The upper curve corresponds to Eq. (2.1) (broken phase), the lower one to Eq. (2.2) (unbroken phase).

Table I. The Critical Points for Various α

α	β_{crit}	α	β_{crit}
0.25	0.1865(5)	1.25	0.269(1)
0.50	0.259(1)	1.50	0.264(1)
0.75	0.274(1)	1.75	0.258(2)
1.00	0.275(1)	2.00	0.253(1)

this to be the case because of the analytical calculation on the $\beta = 1$ line done in ref. 7.

A final test of our picture can be obtained looking at the spectrum of the hamiltonian, which is explicitly given in Appendix B. We consider the first three levels and take $\alpha = 1$ only. Since the ground state has energy zero, the values of the energies of the next two levels, denoted by E_1 and E_2, coincide with the energy gaps. If our picture is correct E_1 should vanish for large values of L for $\beta < \beta_{crit}$ since in the large L limit one needs two states, the ground state and the first excited state, to describe the two vacua.

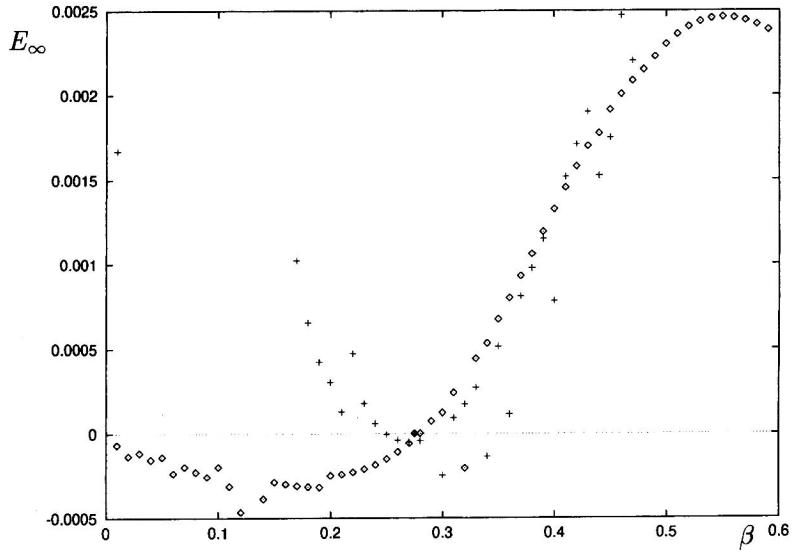

Fig. 6. Estimates of the first (◇) and second (+) excitations of the *CP*-symmetric hamiltonian (Eq. B.1) with $h = 0$). The estimates were obtained using the spectra of the hamiltonian up to eleven sites and extrapolating the results in standard ways. Since all eigenvalues of H are positive the errors of the values shown are estimated to be 0.0003.

E_2 should be finite. For $\beta > \beta_{\text{crit}}$ both E_1 and E_2 should be finite. Using the modified Arnoldi algorithm of ref. 16 we have calculated, for various values of β and chain lengths (up to $L = 11$) the values of E_1 and E_2. In order to get their large L limit we have used Bulirsch–Stoer approximants.[17] The results are shown in Fig. 6 which confirms the existence of a critical point around $\beta = 0.275$. If one takes $\beta = \beta_{\text{crit}}$ one can estimate the dynamical critical exponent z defined as follows:

$$\lim_{L \to \infty} L^z E_1(L) = \text{const.} > 0 \tag{2.3}$$

where $E_1(L)$ represents the energy of the first exited state for a chain of length L. We find $z = 2.0 \pm 0.1$. (A better estimate of z is not possible, since β_{crit} is known only up to three digits.) This result is also interesting because from our experience with the one-species problem (see Appendix A) a value of $z = 2$ suggests the existence of shocks. In the next section we are going to find them.

3. DESCRIPTION OF THE FIRST-ORDER PHASE TRANSITION

We are now going to study in detail the point $\alpha = 1, \beta = \beta_{\text{crit}} = 0.275$ where as explained in the last section we have seen a first-order phase transition. The physics of the steady state can be understood only if one considers the two order parameters p and m.

In Fig. 7 we show, in the $p - m$-plane, the contour lines of the FEF $f_L(p, m)$ near its minima. The figure suggests a large L limit in which we get the following picture: one line segment parallel to the p-axis (from U to V in Fig. 7), one line segment parallel to the m-axis (from S to R), a smooth curve joining the points S, T and U. Let us give the (p, m) coordinates of these five points: $V = (0.725, 0.149)$ where p and m are obtained from the mean-field equation (1.10), $R = (0.149, 0.725)$, obtained from Eq. (1.10) exchanging p and m, $T = (0.216, 0.216)$, obtained from Eq. (1.8). It is convenient to denote by p_A and m_A the p and m coordinates of the point A. With this notation the coordinates of the points U and S are $U = (1 - p_V, m_V)$ and $S = (p_R, 1 - m_R)$. The points V and R are to be expected to play a special role since they represent the broken phase for a value of β slightly smaller than β_{crit}. Also the point T is to be expected since it corresponds to the symmetric phase (β slightly higher than β_{crit}). The points S and U are unexpected since they do not correspond to any phase. Their coordinates have however a remarkable property: $p_U = 1 - p_V$ and similarly $m_S = 1 - m_R$. These relations are typical for shocks (see Appendix A and ref. 12). The following simple model captures the physics of the phase transition. First let us introduce the scaling variable $z = k/L$,

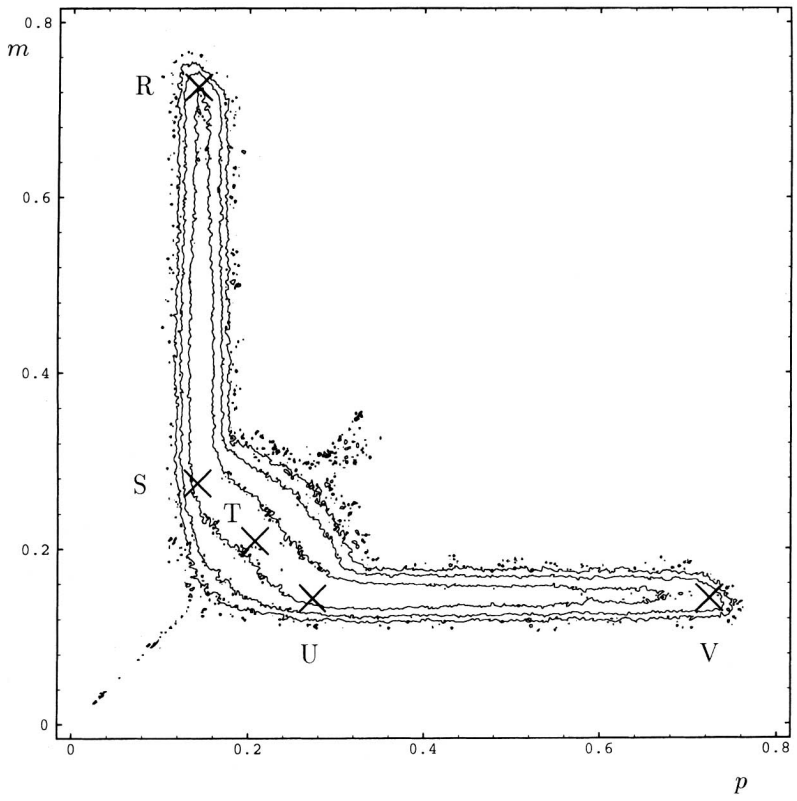

Fig. 7. Contour lines of $f_l(p, m)$ for $\beta = 0.275$ and $L = 1000$ sites. The "height" difference between lines is constant.

where k is the site variable and L the length of the lattice. The model will apply in the limit where k and L are large. We assume that the following processes take place:

- With a probability P_1 we have shocks of uncorrelated positive particles as described by Fig. 8a. The probability to find a positive particle at the left of the point g with a density p_U and to the right of the point g with a density p_V is independent of z. One has fronts for $0 < g < 1$ with equal probability (this corresponds to the U-V line segment). The negative particles are also uncorrelated and have a constant density m_V.

- Also with a probability P_1 we have shocks of negative particles (see Fig. 8b) which are just the *CP*-reflected shocks of the positive particles (this corresponds to the R-S line segment).

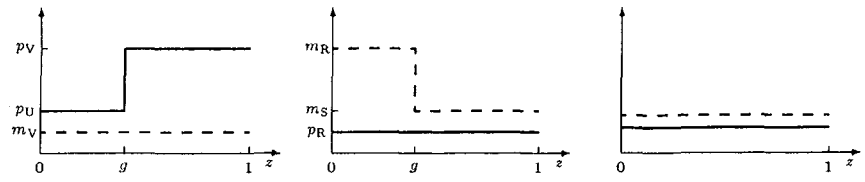

(a) (b) (c)

Fig. 8. The shocks appearing at the first-order phase transition. The solid and broken lines give the profile of positive and negative, respectively.

• With a probability P_2 we have configurations (Fig. 8c) of constant density (independent of z) corresponding to all pairs of values p and m along the line segment S-U, all with the same probability.

Obviously

$$2P_1 + P_2 = 1 \tag{3.1}$$

The assumption that we have a line segment between S and U is an approximation since this line segment intersects the $p = m$ line in the point of coordinates $((p_U + p_R)/2, (m_S + m_V)/2) = (0.212, 0.212)$ which does not coincide with T but is very close to it. We did not try to find a better description of the S-T-U curve because this would imply many more Monte Carlo data than we were able to collect.

The probabilities P_1 and P_2 are determined from the condition that $f_L(p, m)$ has the same value everywhere on the "boomerang." We get

$$P_1 = \frac{p_V - p_U}{2(p_V - m_V)} = 0.39 \tag{3.2}$$

$$P_2 = \frac{p_U - m_V}{p_V - m_V} = 0.22 \tag{3.3}$$

Let us now check the model, in this way we can present the data in an organized way. First, we can compute $f(d)$. One obtains a function which is flat between $-(p_V - m_V)$ and $(p_V - m_V)$. This is just what one sees in Fig. 2 for β_{crit}. Next we compute $m(z)$ and get

$$\begin{aligned} m(z) &= P_1 m_V + \tfrac{1}{2} P_2 (m_V + m_S) + P_1 (m_R - z(m_R - m_S)) \\ &= 0.387 - 0.175z \end{aligned} \tag{3.4}$$

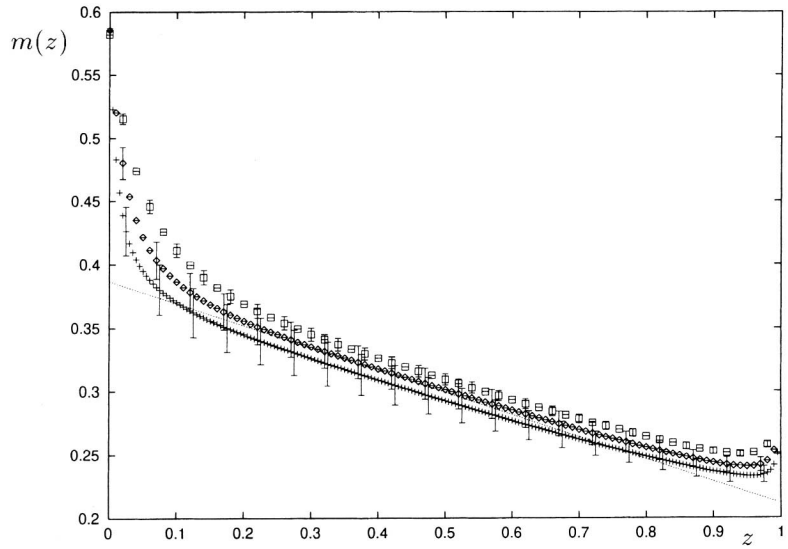

Fig. 9. Density profile of the negative particles for $L = 50$ ($\square$), 100 ($\diamond$), 200 ($+$) at the phase transition $\beta = 0.275$. The straight line is given by Eq. (3.4).

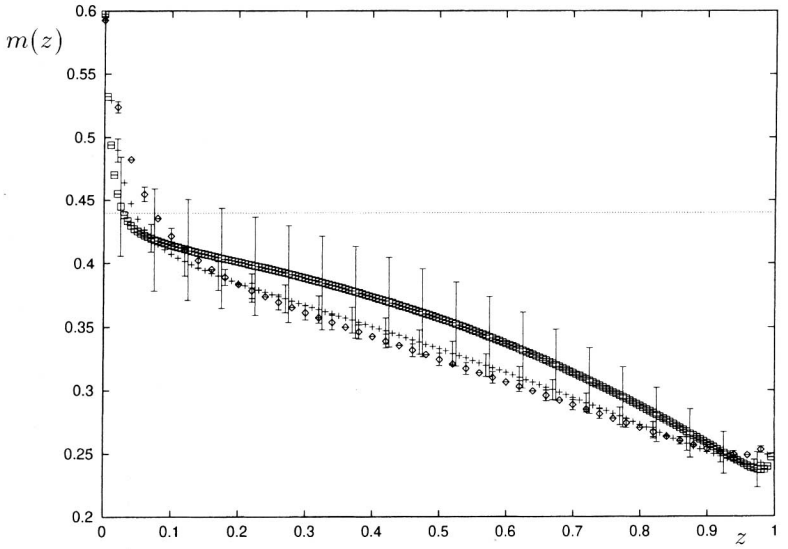

Fig. 10. Density profile of the negative particles for $L = 50$ ($\diamond$), 100 ($+$), 200 ($\square$) at $\beta = 0.26$, below the phase transition. The line gives the mean-field prediction, i.e. the average of the densities of Eq. (1.10).

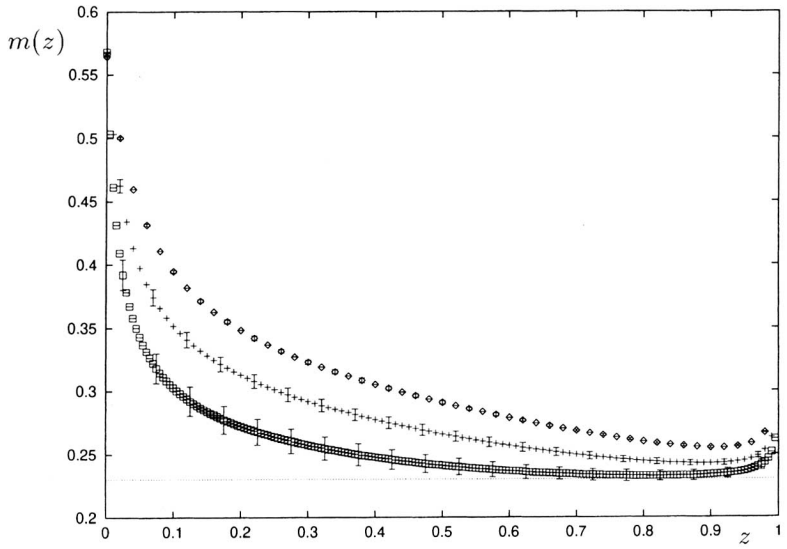

Fig. 11. Density profile of the negative particles for $L=50$ ($\diamond$), 100 ($+$), 200 ($\square$) at $\beta=0.30$, above the phase transition. The line gives the (unstable) mean-field solution (1.8).

Obviously $p(z)=m(1-z)$. In Fig. 9 we show the density of negative particles as a function of z for various numbers of sites. One notices that the straight line given by Eq. (3.4) fits the data.

In order to make sure that the linear density distribution observed in Fig. 9 is not a finite-size effect, in Fig. 10 we show for $\beta=0.26$ (below the critical point) the function $m(z)$. One observes that the data converge (slowly) from below to the mean-field value $m=0.44$ obtained taking the average of the two equations (1.10).

In Fig.11 we show $m(z)$ for $\beta=0.3$ (above β_{crit}). The data converge from above to the value $m=0.23$ which is obtained from Eq. (1.8). In conclusion, the non-constant distributions seen just below and just above β_{crit} are cross-over phenomena.

In order to "see" the shocks, we have looked at configurations where the density of positive particles p, averaged over the lattice, is fixed. This corresponds to a point on the U-V line segment in Fig. 7 and one expects to see a shock like in Fig. 8a. Since we are also interested to see what kind of finite-size effects exist (see Appendix A), we have chosen to present the densities as functions not of z but in terms of the variable

$$y=\frac{k-k_0}{\sqrt{L}} \tag{3.5}$$

where k_0 is the position of the front which in the large L limit is given by

$$k_0 = \frac{L}{2\beta_{\text{crit}} - 1}(p - 1 + \beta_{\text{crit}}) \tag{3.6}$$

The data for $p = 0.5$ are shown in Fig. 12. Let us leave aside for a moment the existence of "tails" on the left hand side of the figure. The data scale, they are independent of L. A good fit to the data is given by

$$p(y) = (\tfrac{1}{2} - \beta_{\text{crit}})\,\text{erf}(y/2) + \tfrac{1}{2} \tag{3.7}$$

Obviously, if we show the data as a function of z one gets the front from Fig. 8a with $g = 0.5$. The value of m in Fig. 12 corresponds to the value of m_V in Fig. 8a as expected. We now turn our attention to the "tails." For the positive particles one can fit the data like

$$p(k) = \mu k^{-1/2} + \beta_{\text{crit}} \tag{3.8}$$

where k is the position of the site starting with the left hand side of the chain and $\mu = 0.08$ is a constant. We have checked that for other shocks (one takes p different of 0.5 but still on the U-V segment of Fig. 7) the value of μ stays unchanged. For negative particles the tails are exponential

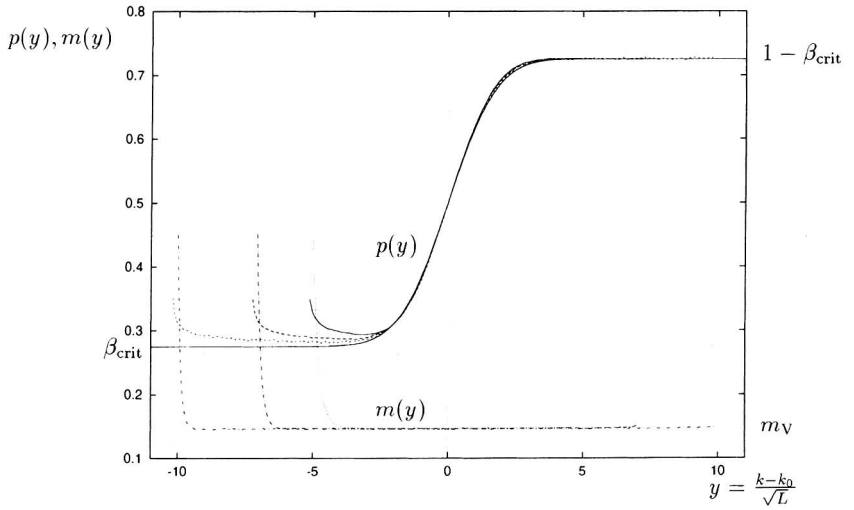

Fig. 12. Scaling of the shock: Density profiles of positive and negative particles for $p = 0.5$ fixed. Data for $L = 100, 200, 400$ sites. The solid curve fitted to the shock is given by Eq. (3.7). Eq. (3.6) gives the expression of k_0.

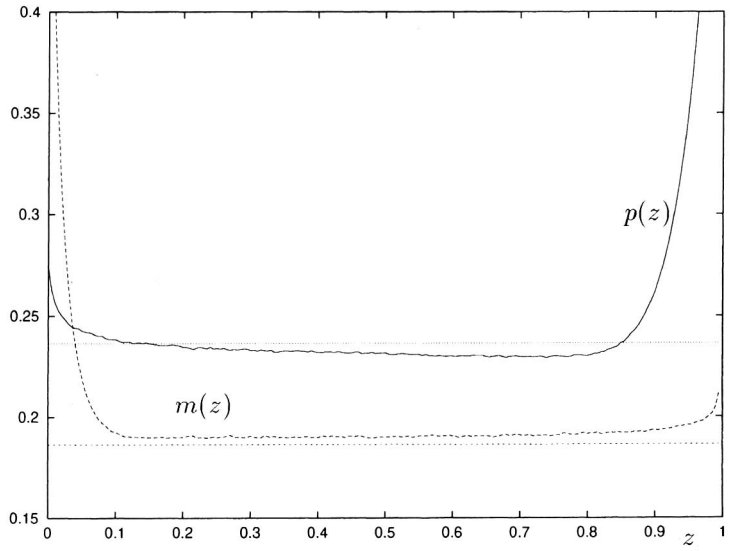

Fig. 13. Density profile $p(z)$ and $m(z)$ for $d=0.05$ and $L=200$.

with a correlation length independent of L. This observation is intriguing because common sense would suggest that in this case one should have a finite correlation length also in the time direction, i.e. masses in the spectrum of the problem and not only the massless excitations discussed in Section 2.

Another test of the model, this time on a part of it on which we certainly expect to be less precise, is to "cut" through the handle of the boomerang. We have taken $d=0.05$ in order to check if profiles like in Fig. 8c are seen. The data are shown in Fig. 13 together with the expected constant values (take the intersection of the line $d=0.05$ with the line segment S-U in Fig. 7). As one notices we find agreement although some mini-shocks are not excluded. After presenting the data we are left with a puzzle. We have expected the point T to be singled out in some way (it represents the symmetric phase), but it is not.

4. THE BROKEN PHASE IN THE PRESENCE OF A SYMMETRY BREAKING EXTERNAL SOURCE

4.1. The Free Energy Functional

As explained in Section 2 and shown in Fig. 14, the phase diagram of the *CP*-symmetric model consists of a power law phase A and a broken

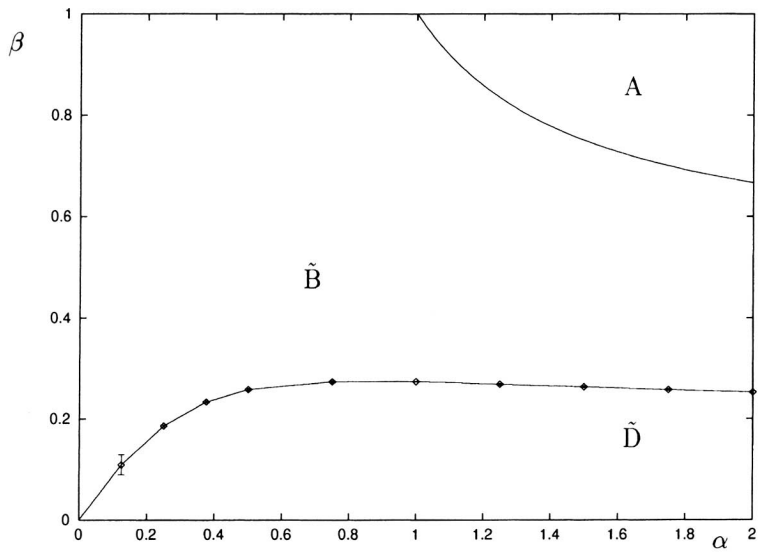

Fig. 14. Phase diagram of the two-species model for $h=0$ obtained from the Monte Carlo simulations. The phase A is given by mean field.

phase $\tilde{D}$ separated by a first-order phase transition line from the unbroken phase $\tilde{B}$. In equilibrium systems, if one has a transition from an ordered to a disordered phase, the broken phase corresponds to first-order phase transitions (and the FEF is a flat function between the two phases). As we have seen this is not the case for steady states and for this reason we use the expression "first-order" only on the separation line where the FEF is flat and the expression "broken phase" for the domain where the FEF is not convex and has two minima.

We consider now the effect of an explicit *CP* symmetry breaking in the model. We take $h>0$ in the boundary rates given by equations (1.2) and (1.3). Using Monte Carlo simulations, we have computed the FEF $f_L(d, h)$ taking $\alpha=1$ and several values of β and h; d is again the difference between the average densities of positive and negative particles. In Fig. 15 we show $f_L(d, h)$ for $\beta=0.1$ (in the $\tilde{D}$ phase) and several values of h. We observe that below $h_{\text{crit}}=0.2281$ the FEF shows two minima and only one minimum for $h>h_{\text{crit}}$. For $h=h_{\text{crit}}$ the first and second derivative of $f_L(d, h)$ with respect to d vanishes. This is the definition of a spinodal point.[15]

The behavior of $f_L(d, h)$ is the one expected from a Ginzburg–Landau ansatz.[18] Our data are of course not precise enough to give an estimate with four digits for h_{crit}, the value we give is obtained in mean-field. We will return soon to the problem of the validity of mean-field.

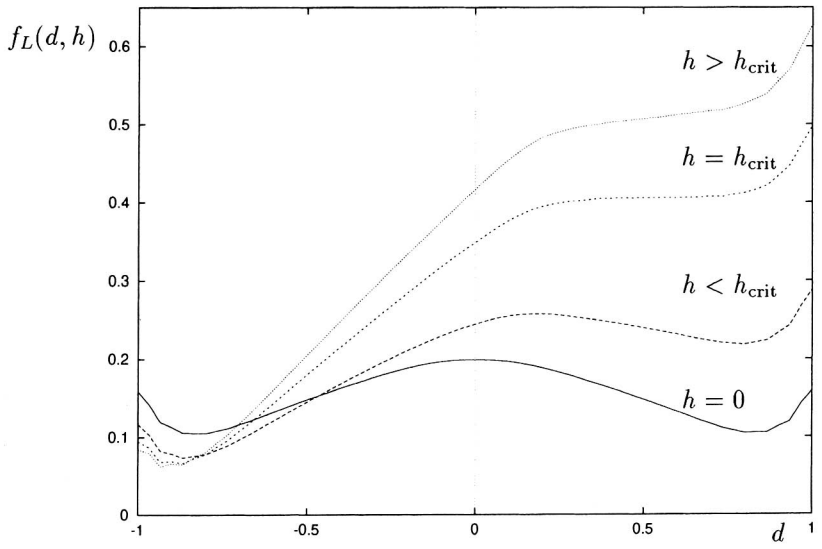

Fig. 15. $f_L(d, h)$ for $L = 30$, $\alpha = 1.0$, $\beta = 0.1$ and $h = 0.1, 0.2281, 0.3$. For $h = 0$ the system is in the phase $\tilde{D}$.

In the Ginzburg–Landau ansatz $f(d, h)$ has a simple h dependence:

$$f(d, h) = f(d, h = 0) + vhd + g(h) \tag{4.1}$$

where v is a parameter. We have collected data for various values of β and h and find $v = 1.4$ getting a fit to the data within 10%. In Fig. 16 we fix the value of $h = 0.02$ and show the difference

$$f_L(d, h = 0) - f_L(d, h = 0.02) \tag{4.2}$$

as a function of d. According to Eq. (4.1) we expect straight lines with the slope -0.028. The data are compatible with this prediction. We have repeated the simulations for several values of h with the same result.

4.2. Validity of the Mean Field Approximation

We have computed the mean-field approximation of the model (1.1–1.3) for h different from zero (see Appendix C), extending the calculation done in ref. 7. Our motivation was to find out if, like in the $h = 0$ case, one can understand in a simple way where and in which way mean-field is exact or wrong. In Table II, for different values of β and h, we give the

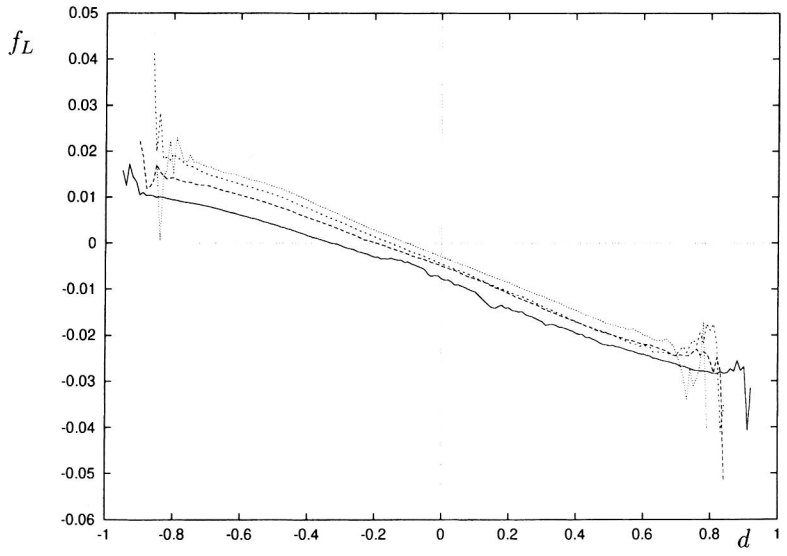

Fig. 16. $f_L(d, h=0) - f_L(d, h=0.02)$ for $\beta = 0.20, 0.26, 0.28, 0.30$ and $L = 100$ sites.

values of $d_L^{\min}$ which denotes the minima of the FEF as determined by Monte Carlo simulations as well as the values of $d_{\mathrm{m-f}}$ obtained in mean-field. Comparing the Monte-Carlo simulations with the mean-field results we reach the conclusion that probably mean-field is not exact anywhere. It remains, however, a good approximation for small values of β and large values of h.

4.3. The Dynamical Critical Exponent at the Spinodal Point

We are now going to discuss some aspects of the dynamics of the model when one includes the symmetry breaking term. Our attention goes first to the spinodal point and we look at the spectrum of the hamiltonian (see Appendix B). We notice that the first excited state has an energy which vanishes in the large L limit. The dynamical critical exponent (see Eq. (2.3)) determined using the values of the first excited state of chains up to 11 sites $\beta = 0.1$ and $h_{\mathrm{crit}} = 0.22810$ as given by mean-field is $z = 1.00 \pm 0.01$. We have repeated the same calculation for $\beta = 0.05$ ($h_{\mathrm{crit}} = 0.28096$) and found $z = 1.000 \pm 0.001$. (Notice that we have taken small values of β and that the values of h_{crit} are large.)

From previous experience with quantum chains,[28] for a three-state model 11 sites are enough for a reasonable estimate of the asymptotic behaviour of energy gaps if the critical point is known. In order to check

Table II. The Minima $d_L^{\min}$ of $f_L(d)$ (Error ± 0.01) and the Mean-Field Predictions d_{m-f} for $\alpha = 1$, Various β and h[a]

β	h	L	$d_L^{\min}$	d_{m-f}
0.6	0	200	**0.00**	0
	0.1	200	**−0.08**	−0.0943
0.35	0	400	**0.00**	0
	0.02	100	−0.05	−0.468
	0.1	100	−0.45	−0.512
0.329	0	400	0.00	−0.490/+0.490/0
	0.02	200	−0.06	−0.501
	0.1	200	**−0.52**	−0.543
0.3	0	400	0.00	−0.537/+0.537/0
	0.02	400	−0.15	−0.546/+0.527/+0.098
	0.1	400	**−0.58**	−0.584
0.26	0	200	**−0.53/+0.53**	−0.600/+0.600/0
	0.01	100	**−0.53**/+0.43	−0.604/+0.596/+0.019
	0.02	100	**−0.54**	−0.607/+0.592/+0.038
	0.07	100	**−0.61**	−0.629
0.1	0	200	**−0.84/+0.84**	−0.849/+0.849/0
	0.02	100	**−0.84/+0.84**	−0.852/+0.846/+0.00519
	0.05	100	**−0.85/+0.83**	−0.856/+0.841/+0.013
	0.1	50	**−0.86/+0.81**	−0.864/+0.833/+0.026

if the mean field estimates of h_{crit} are correct, we have computed the connected two-point function in the bulk using Monte-Carlo simulations. It is indeed zero. To our knowledge it is for the first time that the exponent $z = 1$ appears in stochastic processes.

In ref. 19 the toy-model of Godrèche *et al.*[20] is examined (which corresponds to the $\beta \to 0$ limit of the present model) and again $z = 1$ is found. More than that, in ref. 19 it is shown that the spectrum has massless excitations which are universal and also massive excitations. (As opposed to the present model where we could study properly only one level, in the toy-model we can study many of them.) The toy-model has two parameters, one which corresponds to α in the original model and h. Normalizing the hamiltonian such that the sound velocity is the same, at the spinodal point

the spectra corresponding to the massless regime do not depend on the former parameter.

One can ask which implications has a $z = 1$ exponent. Since in stochastic processes one computes quantities which correspond in field theory to form factors and not to vacuum expectation values, the application of ideas coming from conformal invariance as suggested by $z = 1$ are not obvious. In ref. 19 several properties of the time dependence of the order parameter are given. The simplest one being that the flip time[6] from a configuration with the d value of the spinodal point to a configuration corresponding to the minimum of $f_L(d, h)$ (see Fig. 15) should be proportional to L.

4.4. Flip Time and Barriers of the Free Energy Functional

We would like to make an observation on the flip times related to barriers in the FEF. Let us take $\beta = 0.1$ and $h = 0.1$ in Fig. 15 and denote by $\Delta_1(\Delta_2)$ the difference between the maximum of the FEF and the minimum of the FEF for negative (positive) values of d ($\Delta_2 = 0$ at the spinodal point). From the Monte Carlo data ($L = 50$ sites) we get $\Delta_1 = 0.178 \pm 0.002$ and $\Delta_2 = 0.041 \pm 0.002$. The two flip times from the stable (unstable) to the unstable (stable) phase are T_{long} (T_{short}). They have been measured for

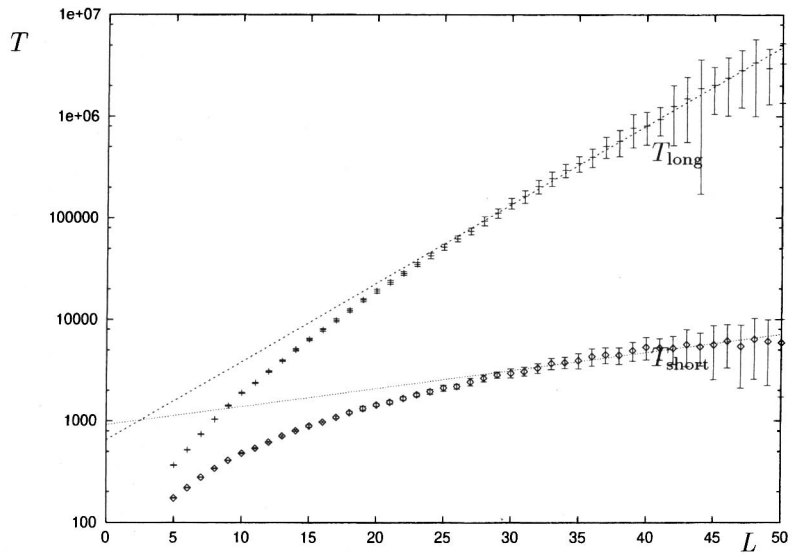

Fig. 17. Logarithmic plot of the flip times for $\alpha = 1.0$, $\beta = 0.1$ and $h = 0.1$. The dotted curves are given by (4.3).

chains of different lengths L and their values are shown in Fig. 17. The straight lines in Fig. 17 are given by the ansatz

$$\begin{aligned} T_{\text{long}} &\propto \exp(\Delta_1 L) \\ T_{\text{short}} &\propto \exp(\Delta_2 L) \end{aligned} \tag{4.3}$$

The agreement between the ansatz (4.3) and the data shows a connection between the dynamics of the model (flip times) and the properties of the steady state (the FEF). Repeating the same procedure for a different value of gives the same result. More about this subject can be found in ref. 19.

5. CONCLUSIONS

We have shown in the framework of the two-species model the following pattern of spontaneous CP symmetry breaking for steady states. If we start in the "disordered" phase (where the free energy functional as a function of the order parameter has only one minimum) and lower the "temperature" (the parameter β) we have a first-order phase transition at β_{crit} with a flat free energy functional (like in equilibrium problems). At β_{crit} the density profiles and correlation functions in the scaling regime can be explained using a certain combination of shocks. Below the critical "temperature" β_{crit}, in the broken phase, the free energy functional is not a convex function of the order parameter (unlike in equilibrium problems) but has two minima corresponding to two phases defined by their average densities of positive and negative particles. If the CP symmetry of the model is broken by a small perturbation (parameter h), one has only one minimum for the first-order phase transition (like in equilibrium) but still two minima in the broken phase. If we increase h one gets spinodal points.

At the first-order phase transition we have seen massless excitations in the spectrum of the quantum chain hamiltonian associated with the dynamics of the process with a critical dynamical exponent $z = 2$. This does not exclude the presence of massive excitations which are suggested by the exponential tails seen in Fig. 9 and Fig. 12 in the density profiles. Massive excitations are not seen for the one-species model described in Appendix A.[21]

At the spinodal points we have also seen massless excitations with $z = 1$ as well as massive excitations. The latter are suggested by exponential tails observed in the density profiles not shown in this paper. These observations are confirmed by the investigation of the low β limit of the model.[19] At this point it is not clear if the exponent $z = 1$ has profound implications like in equilibrium problems where it implies conformal invariance or is just one dynamical critical exponent among others. We

have looked to conformal towers in the spectrum of the hamiltonian but the data of our short quantum chains did not give any clean results. This is probably due to the fact that the critical point is not known exactly (we used the values obtained from mean-field) and that in general the convergence to the thermodynamic limits is slower in stochastic quantities than in equilibrium ones. This is an empirical observation. We think that a further investigation of the model is necessary by taking the second rate in (1.1) not equal to the other two. Some preliminary results are described in ref. 7. This study can be done not only by Monte Carlo simulations but also using the analytical methods developed recently in ref. 22.

APPENDIX A. THE ASYMMETRIC EXCLUSION PROCESS

The physics of this model is well understood,[2–4] here we are going to discuss some aspects of it which are necessary for the understanding of the finite-size effects of the two-species model. We consider a chain of length L with two types of particles ($+$ and $-$). In an infinitesimal time step dt the following processes take place:

$$\begin{aligned} (+)_k(-)_{k+1} &\to (-)_k(+)_{k+1} \quad \text{with probability } dt \\ (-)_1 &\to (+)_1 \quad \text{with probability } \alpha\, dt \\ (+)_L &\to (-)_L \quad \text{with probability } \beta\, dt \end{aligned} \tag{A.1}$$

Defining $\sigma = \alpha + \beta$ and $h = \beta - \alpha$ one notices that for $h = 0$ the model is *CP*-invariant. We denote by c the average density of positive particles. The model presents three phases:

- the power law phase ($\alpha > 1/2, \beta > 1/2$) where $c = 1/2$
- the low density phase ($\alpha < 1/2, \beta > \alpha$) where $c = \alpha$
- the high density phase ($\alpha > \beta, \beta < 1/2$) where $c = 1 - \beta$

A coexistence line ($\alpha = \beta < 1/2$) separates the low density from the high density phase. The concentration has a discontinuity along this line from $c = \beta$ to $c = 1 - \beta$.

Using Monte Carlo simulations we have computed the FEF $f_L(c, h)$ keeping σ A fixed and using several values of h. The results are shown in Fig. 18. We notice that for $h = 0$, the FEF is a flat function between $c = \beta$ and $c = 1 - \beta$. A small positive $h(h = 0.004)$ gives a FEF with only one minimum at $c = \beta$ just like in equilibrium first-order phase transitions. A larger value of h ($h = 0.1$) moves the minimum away. We have studied the convergence of the function $f_L(c, h)$ to $f(c, h)$ taking $c_{\min}$ the value of c where

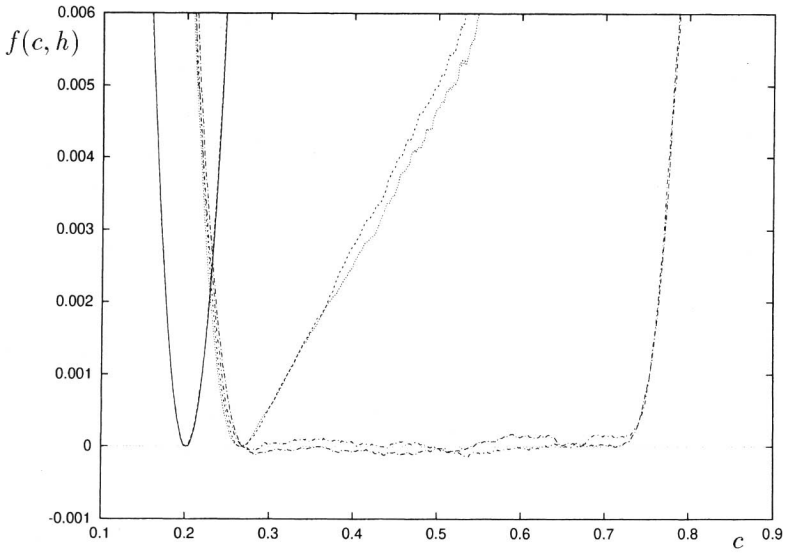

Fig. 18. Asymmetric diffusion model: $f_L(c,h)$ for $s=0.25$ and $h=0, 0.004, 0.5$, each for $L=600$, 800 and 1000 sites. We substracted $f_L(c_{\min},h)$ from each curve.

the FEF has a minimum. For all the examples we have studied we have found that

$$f_L(c_{\min},h)=f(c_{\min},h)+a/L \tag{A.2}$$

Where the constant a depends on σ and h. For example if we take $\sigma=0.5$ and $h=0.2$ like in Fig. 18 we find $a=4.2\pm0.2$. We have also found that if we start on the coexistence line with a certain value of σ and switch-on the *CP* symmetry breaking term h, we have the following simple expression for the FEF:

$$f(c,h)=f(c,h=0)+vch+g(h) \tag{A.3}$$

where v depends on σ. For the example $\sigma=0.5$ studied above we find $v=4.5$. We have observed that if we take $L=200$ the FEF has already a shape independent of L, the single L dependence being in $f_L(c_{\min},h)$.

We would like to mention that much of the physics which will be described below is contained in a simplified model studied by Schutz.[23] In this model the bulk dynamics is deterministic and only the boundaries are stochastic. The critical dynamical exponent on the coexistence line of the present model is $z=2$[21] like in ref. 23. This corresponds to the picture in which the front of a shock performs a symmetric random walk.

On the coexistence line the density of positive particles is high at the right hand side of the chain ($c = 1 - \beta$) and low at the left hand side of the chain ($c = \beta, \beta < 1/2$). The two regimes are joined by a shock front. One measures such a shock by constraining the average density of positive particles to a given value between β and $1 - \beta$. If $c(k)$ is the concentration at lattice site k, it is useful to define the variable

$$y = \frac{k - k_0}{\sqrt{L}} \tag{A.4}$$

where

$$k_0 = \frac{L}{2\beta - 1}(c - 1 + \beta) \tag{A.5}$$

is the position of the shock front. In Fig. 19 we show the Monte Carlo data for $c = 0.5$ and $\alpha = \beta = 0.25$. The existence of a front with width of order $L^{1/2}$ is to be expected from the model studied by Schutz,[23] from the exclusion model with a blockage[24, 25] and from the asymmetric model with an

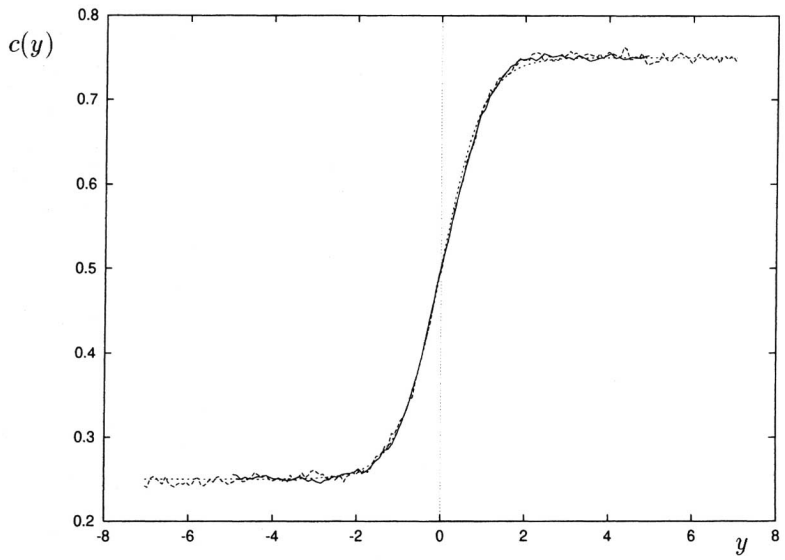

Fig. 19. Scaling of the shock: Density profiles for $\alpha = \beta = 0.25$ (with $c = 0.5$ fixed) and for $L = 100, 200$. The dotted curve is given by Eq. (A.6). The wriggled curves represent the Monte Carlo data which coincide with Eq. (A.6) within 1%.

impurity,[26] and by some other models considered in ref. 27. These models suggest the following expression for the front profile:

$$c(y)=\frac{1}{2}+\left(\frac{1}{2}-\beta\right)\operatorname{erf}\left(\frac{1-2\beta}{\sqrt{2\beta(1-\beta)}}\,y\right) \tag{A.6}$$

The Monte Carlo data are fitted within 1% by this function.

Our purpose in studying the finite-size behavior of the shocks was to find out how many lattice sites are necessary to be in the scaling limit in order to know for the threestates model which lattice size are necessary to see shocks. It turns out that $L=100$ are enough.

APPENDIX B. THE HAMILTON OPERATOR

The time evolution operator H of the master equation (1.4) for the processes (1.1)–(1.3) can be written as a sum of operators acting non-trivially on adjacent sites only (hopping) and of two operators acting on the first and last site (input and output):[8]

$$H=H_1+\sum_{k=1}^{L-1} H_{k,k+1}+H_L \tag{B.1}$$

The matrices are

$$H_{k,k+1}=I_1\otimes\cdots\otimes I_{k-1}\otimes\begin{pmatrix}
0&0&0&0&0&0&0&0&0\\
0&0&0&-1&0&0&0&0&0\\
0&0&1&0&0&0&0&0&0\\
0&0&0&1&0&0&0&0&0\\
0&0&0&0&0&0&0&0&0\\
0&0&0&0&0&1&0&0&0\\
0&0&-1&0&0&0&0&0&0\\
0&0&0&0&0&-1&0&0&0\\
0&0&0&0&0&0&0&0&0
\end{pmatrix}_{k,k+1}$$

$$\otimes I_{k+2}\otimes\cdots\otimes I_L$$

$$H_1=\begin{pmatrix}
\alpha&0&-\beta(1-h)\\
-\alpha&0&0\\
0&0&\beta(1-h)
\end{pmatrix}_1\otimes I_2\otimes\cdots\otimes I_L$$

$$H_L=I_1\otimes\cdots\otimes I_{L-1}\otimes\begin{pmatrix}
\alpha&-\beta(1+h)&0\\
0&\beta(1+h)&0\\
-\alpha&0&0
\end{pmatrix}_L$$

where the subscripts denotes the sites the matrices act on and I is the 3×3 unit matrix. The order of the basis at each site is chosen as $|0\rangle, |+\rangle, |-\rangle$. Note that H is not hermitian.

APPENDIX C. MEAN-FIELD THEORY FOR $H > 0$

In this appendix we present the extension of the mean-field theory[7] to the $h > 0$ case. The time evolution of the average values of the densities is given by the following equations

$$\begin{aligned}
&\frac{\mathrm{d}}{\mathrm{d}t} p(1) = \alpha(1 - p(1) - m(1)) - p(1)(1 - p(2)) \\
&\frac{\mathrm{d}}{\mathrm{d}t} p(k) = p(k-1)(1 - p(k)) - p(k)(1 - p(k+1)) \\
&\qquad\qquad \text{for} \quad k = 2, 3, \ldots, L-1 \\
&\frac{\mathrm{d}}{\mathrm{d}t} p(L) = p(L-1)(1 - p(L)) - \beta(1+h)\, p(L) \\
&\frac{\mathrm{d}}{\mathrm{d}t} m(1) = m(2)(1 - m(1)) - \beta(1-h)\, m(1) \\
&\frac{\mathrm{d}}{\mathrm{d}t} m(k) = m(k+1)(1 - m(k)) - m(k)(1 - m(k-1)) \\
&\qquad\qquad \text{for} \quad k = 2, 3, \ldots, L-1 \\
&\frac{\mathrm{d}}{\mathrm{d}t} m(L) = \alpha(1 - p(L) - m(L)) - m(L)(1 - m(L-1))
\end{aligned} \tag{C.1}$$

For the stationary state one takes the left hand sides of Eqs. (C.1) equal to zero. The resulting equations can be written as the condition that the current of the positive and negative particles is site-independent:

$$j^+ = \alpha(1 - p(1) - m(1)) = p(k)(1 - p(k+1)) = \beta(1+h)\, p(L) \tag{C.2}$$

$$j^- = \beta(1-h)\, m(1) = m(k)(1 - m(k-1)) = \alpha(1 - p(L) - m(L)) \tag{C.3}$$

Notice that in the bulk the equations for $p(k)$ and $m(k)$ decouple. It is convenient to denote

$$\beta^{\pm} = \beta(1 \pm h) \tag{C.4}$$

$$\alpha^{+} = \frac{\alpha(1 - p(1) - m(1))}{1 - p(1)} = \frac{j^{+}}{j^{+}/\alpha + j^{-}/\beta^{-}} \tag{C.5}$$

$$\alpha^{-} = \frac{\alpha(1 - p(L) - m(L))}{1 - m(L)} = \frac{j^{-}}{j^{-}/\alpha + j^{+}/\beta^{+}} \tag{C.6}$$

The problem of solving equations (C.2) and (C.3) is reduced to solving two models each with one type of totally asymmetric diffusing particles and with input and output rates α^{+}, β^{+} and α^{-}, β^{-} respectively. The solution of the latter problem is known.[2-4] Each of the decoupled chains is in one of the phases of the asymmetric diffusion model. Depending on α, β and h, only certain combinations of phases can occur, since the two chains are coupled through the boundaries (C.5) and (C.6).

Let us first consider the phases of the two-species model where the current of positive particles equals the current of negative particles, $j^{+} = j^{-}$. In this case equations (C.5) and (C.6) simplify to

$$\alpha^{+} = \frac{\alpha\beta^{-}}{\alpha + \beta^{-}} \tag{C.7}$$

$$\alpha^{-} = \frac{\alpha\beta^{+}}{\alpha + \beta^{+}} \tag{C.8}$$

One finds

◦ *the power-law symmetric phase*

In this phase both currents are $j^{s} = 1/4$ and the densities of the particles is $\rho^{s} = 1/2$. We find this phase for

$$\alpha^{s} > 1/2, \qquad \beta^{s} > 1/2 \tag{C.9}$$

These conditions reduce to

$$\beta > \frac{1}{1-h}\frac{\alpha}{2\alpha - 1}, \qquad \alpha > 1/2 \tag{C.10}$$

This corresponds to the regions A* in Fig. 20 which shows the phase diagram obtained in mean field approximation for $h = 0.1$.

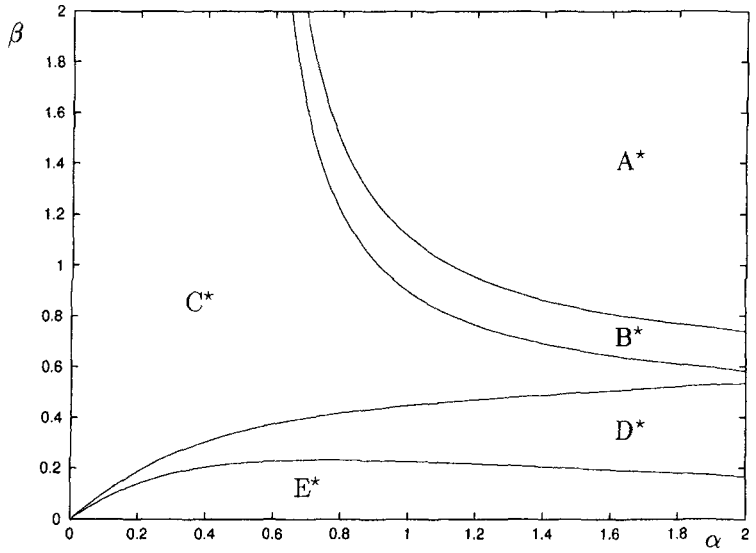

Fig. 20. Mean-field phase diagram for asymmetry $h = 0.1$.

◦ *the low-density symmetric phase*

For $h = 0$ there exists a symmetric low-density phase (B) with $j^+ = j^-$. The conditions for this phase are

$$\alpha^s < 1/2, \qquad \alpha^s < \beta^s \tag{C.11}$$

If we turn on the asymmetry h, this phase does not exist anymore. Instead, one still finds a phase with the two types of particles in the low-density phase of the single-species chain but with different currents. One has to distinguish between the favoured and unfavoured low-density/low-density phase.

◦ *the favoured low-density/low-density phase*

A positive h favours the output of positive particles, such that more negative particles can be injected. Therefore the current of negative particles is more likely to be bigger than the current of positive particles. For the existence of the favoured low-density/low-density phase we have

$$j^+ = \alpha^+(1-\alpha^+) < j^- = \alpha^-(1-\alpha^-) \tag{C.12}$$

and need a solution of (C.5) and (C.6), which can be rewritten as

$$\alpha^+ = 1 - \frac{1}{\alpha}\alpha^+(1-\alpha^+) - \frac{1}{\beta^-}\alpha^-(1-\alpha^-) \tag{C.13}$$

$$\alpha^- = 1 - \frac{1}{\alpha}\alpha^-(1-\alpha^-) - \frac{1}{\beta^+}\alpha^+(1-\alpha^+) \tag{C.14}$$

with

$$\begin{aligned} &\alpha^+ < 1/2, \qquad \alpha^- < 1/2 \\ &\beta^+ > \alpha^+, \qquad \beta^- > \alpha^- \\ &\alpha^- > \alpha^+ \end{aligned} \tag{C.15}$$

This gives the region C* of Fig. 20.

◦ *The unfavoured low-density/low-density phase*

occupies the smaller region E* in the phase diagram and can be found where a solution of (C.13) and (C.14) under the conditions (C.15) with $\alpha^+ > \alpha^-$ instead of $\alpha^- > \alpha^+$ exists. The respective region in the phase diagram shrinks with increasing h, since the asymmetry favours the other low-density/low-density phase.

◦ *The favoured high-density/low-density phase*

is the phase where the negative particle is in the high-density phase, since the input of negative particles is favoured and it is more probable to find a high density of negative particles. The positive particles are in the low-density phase and we have

$$j^+ = \alpha^+(1-\alpha^+), \qquad j^- = \beta^-(1-\beta^-) \tag{C.16}$$

The solution of (C.5) and (C.6) has to fulfill

$$\alpha^+ < 1/2, \qquad \beta^- < 1/2 \tag{C.17}$$

$$\beta^+ > \alpha^+, \qquad \beta^- < \alpha^- \tag{C.18}$$

This gives the regions D* and E* of Fig. 20.

◦ *The unfavoured high-density/low-density phase*

In this case one has

$$j^+ = \beta^+(1-\beta^+), \qquad j^- = \alpha^-(1-\alpha^-) \tag{C.19}$$

and the conditions

$$\beta^+ < 1/2, \qquad \alpha^- < 1/2 \tag{C.20}$$

$$\alpha^+ > \beta^+, \qquad \alpha^- < \beta^- \tag{C.21}$$

These conditions are fulfilled in region E*.

For $\beta \to 0$ equations (C.20) and (C.21) can be replaced by

$$h < \frac{1}{1+2\alpha} \tag{C.22}$$

◦ *The low-density/power-law phase*

This phase does not occur in the original model with $h = 0$. But for $h > 0$ one finds a phase where the negative particle is in the power-law phase and the positive is in the low-density phase. The conditions are

$$\alpha^+ < 1/2, \qquad \alpha^- > 1/2 \tag{C.23}$$

$$\beta^+ > \alpha^+, \qquad \beta^- > 1/2 \tag{C.24}$$

and give B* in Fig. 20.

Note, that in E* three different stationary solutions of (C.1) are allowed: the unfavoured low-density/low-density and the favoured and unfavoured high-density/low-density phases. However, only the favoured high-density/low-density phase is a dynamically stable solution of (C.1). Increasing the asymmetry region E* shrinks, whereas the regime D* grows.

ACKNOWLEDGMENTS

We would like to thank M. Evans, C. Godrèche, J. M. Luck, D. Mukamel and especially B. Derrida for discussions. We would like also to thank SISSA for hospitality. The work of P. F. A. and T. H. was supported by the DAAD programme HSP II-AUFE. V. R. acknowledges partial support by the EC TMR programmer grant FMRX-CT96-0012.

REFERENCES

1. J. Krug, *Phys. Rev. Lett.* **67**:1882 (1991).
2. B. Derrida, E. Domany, and D. Mukamel, *J. Stat. Phys.* **69**:667 (1992).
3. B. Derrida, M. R. Evans, V. Hakim, and V. Pasquier, *J. Phys. A: Math. Gen.* **26**:1493 (1993).
4. G. Schutz and E. Domany, *J. Stat. Phys.* **72**:277 (1993).

5. P. P. Martin, *Potts models and related problems in statistical mechanics* (World Scientific, Singapore).
6. M. R. Evans, D. P. Foster, C. Godrèche, and D. Mukamel, *Phys. Rev. Lett.* **74**:208 (1995).
7. M. R. Evans, D. P. Foster, C. Godrèche, and D. Mukamel, *J. Stat. Phys.* **80**:69 (1995).
8. F. H. L. Eßler, and V. Rittenberg, *J. Phys. A: Math. Gen.* **29**:3375 (1996).
9. S. Sandow, *Phys. Rev.* **E50**:2660 (1994).
10. R. B. Griffiths, C. -Y. Weng, and J. S. Langer, *Phys. Rev.* **149**:301; J. D. Gunton, M. San Miguel, and P. S. Sahni, in *Phase Transitions and Critical Phenomena*, C. Domb and J. L. Lebowitz, eds. (Academic Press), Vol. 8, p. 267, 1989.
11. M. den Nijs, in *Proceedings of the 4th workshop on Statistical Physics, Seoul, January 27–31* (1997).
12. J. L. Lebowitz, E. Presusti, and H. Spohn, *J. Stat. Phys.* **51**:841 (1988).
13. K. Mallick, Ph.D. thesis, Saclay (1996).
14. C. H. Bennett and G. Grinstein, *Phys. Rev. Lett.* **55**:657 (1985).
15. V. Privman and L. S. Schulman, *J. Phys. A: Math. Gen.* **15**:L238 (1982), and *J. Stat. Phys.* **29**:205.
16. U. Bilstein, diploma thesis, BONN-IB-96-33 (1996).
17. R. Bulirsch and J. Stoer, *Numer. Math.* **6**:413 (1964), M. Henkel and G. Schütz, *J. Phys. A: Math. Gen.* **21**:2617 (1988).
18. M. Le Bellac, *Quantum and statistical field theory* (Oxford University Press, Oxford, 1991).
19. P. F. Arndt and T. Heinzel, cond-mat 9710287 (1997).
20. C. Godrèche, J. M. Luck, M. R. Evans, D. Mukamel, S. Sandow, and S. R. Speer, *J. Phys. A: Math. Gen.* **28**:6039 (1995).
21. U. Bilstein and B. Wehefritz, *J. Phys. A: Math. Gen.* **30**:4925 (1997).
22. F. C. Alcaraz, S. Dasmahapatra, and V. Rittenberg, cond-mat 9705172 (1997).
23. G. Schütz, *Phys. Rev.* **E47**:4265 (1993).
24. S. A. Janowsky and J. L. Lebowitz, *Phys. Rev.* **A45**:618 (1992).
25. G. Schütz, *J. Stat. Phys.* **71**:471 (1993).
26. K. Mallick, *J. Phys. A: Math. Gen.* **29**:5375 (1996).
27. K. Krebs, to be published (1997).
28. G. von Gehlen and V. Rittenberg, *J. Phys. A: Math. Gen.* **19**:L625 (1986).